

CFD PREDICTION AND MODEL EXPERIMENT ON SUCTION VORTICES IN PUMP SUMP

Tomoyoshi Okamura,*¹ Kyoji Kamemoto,² and Jun Matsui³

*¹ Department of Mechanical Engineering, Yokohama National University
79-5 Tokiwadai, Hodogaya-ku, Yokohama-city 240-8501, Japan
Tel: +81-45-339-3882 / FAX: +81-45-339-3882
E-mail: okamu@ynu.ac.jp

² Department of Mechanical Engineering, Yokohama National University
79-5 Tokiwadai, Hodogaya-ku, Yokohama-city 240-8501, Japan

³ ditto

ABSTRACT

The sump size is being reduced in order to lower the construction costs of urban drainage pump stations in Japan. As a result of such size reductions, undesirable vortices such as air-entrained and submerged vortices are apt to appear in sumps because of the higher flow velocities. The Turbomachinery Society of Japan (TSJ) Standard S002:2005 states that the appearance of such visible vortices is not permissible for conventional sumps, and experiments with scale models usually have been done to assess the performance of sumps. Such tests, however, are expensive and time-consuming, and therefore, alternative computational fluid dynamics (CFD) methods for evaluating sump performance are desirable. The Research Committee on Pump Sump Model Testing, which is an organization in the TSJ, carried out a benchmark for flows in model sumps. They contributed commercial CFD codes such as “Virtual Fluid System 3D”, “Star-CD 3.22”, “Star-CD 3.26”, and “ANSYS CFX 10.0”. Some of the benchmark results were reported by Matsui, J. at the 23rd IAHR Symposium in Yokohama, Oct 2006. The remaining results comprise this second paper. The calculated results were compared with experimental ones for flow patterns, locations of vortices, and their vorticity. In the experiments, the critical submergences for flow rates were minutely examined through visual observation with a video camera. The locations of the vortices were obtained by using the laser light sheet visualization method. The velocity and vorticity distribution in the sump were measured by using a PIV method. The following results were obtained. 1) The critical submergence for the air-entrained vortex is almost proportional to the flow rate in the sump. The vortex behavior is unsteady and the duration of the vortex varies greatly. 2) The submerged vortex appears accompanying the air-entrained vortex in the region of low submergences and high flow rates. The critical submergence for the submerged vortex is also proportional to the flow rate. 3) Some CFD codes can predict the visible vortex occurrence and its location for submergence and flow rate conditions with enough accuracy for industrial use. 4) The calculated velocity distribution at the bell entrance qualitatively agrees with the experimental results. However, the agreement is poor in terms of the magnitude and distribution patterns of the vorticity. This difference is caused by the lack of accuracy of the experiment and CFD computation. 5) Predicting the critical submergence for the visible vortices was not imposed in the benchmark. The calculated stream lines and vortex core lines are not able to be used to predict the visible vortices with much accuracy. An additional post-processing such as obtaining the vortex core static pressure and comparing it with ambient pressure for an air-entrained vortex or with the saturated vapor pressure of the water for a submerged vortex would be necessary to predict the visible vortices.

Keywords: *Vortex, Suction sump, Pump intake, CFD, PIV, Standard*

NOMENCLATURE

H: Water level, mm,

LLS: Laser light sheet,

PIV: Particle image velocimetry,

Q: Flow rate, m³/min,

T1: Continuous vortex generating period (See Fig. 7),

T2: Continuous vortex duration (See Fig. 7),

x: Ordinate, mm (See Fig. 1),

y: Ordinate, mm (See Fig. 1),

u: Flow velocity component in x direction, m/s,

v: Flow velocity component in y direction, m/s,

w: Flow velocity component in z direction, m/s,

ω: Vorticity, 1/s

1. INTRODUCTION

A rise in the awareness of the need to contain construction costs had led to a significant reduction in the size of pump systems in Japan. Such smaller systems, however, are often affected by undesirable vortices such as air-entrained vortices or submerged vortices because they have higher flow velocities. According to the Japanese TSJ Standard (2004), the appearance of such vortices is not permissible for ordinary pump sumps, and experiments with scale models usually have been performed to assess the performance of a sump or to improve the design of one. However, such endeavors are expensive and time-consuming, and therefore, alternative methods for evaluating sump performance are desirable. In particular, computational fluid dynamics (CFD) techniques have been applied to design higher performance fluid machinery, so the CFD method may be a suitable alternative. Rajendran (1998) and Ansar (2002) used a few CFD computations to predict the flow and the number, location and vorticity of individual vortices in the pump sump, and they obtained good agreement between their computations and experiments. In the future, the CFD technique is expected to become a standard way to assess the number, frequency, and intensity of vortices in pump sumps. The research committee on pump sump model testing of the Turbomachinery Society of Japan recently surveyed the state of the art concerning CFD simulations of flows and vortices in pump sumps. The committee established the first benchmark study for flows and vortices in model sumps in 2004. Okamura (2005) presented the CFD results of the benchmark. That benchmark study does not compare the computational results with the experimental ones, because the experimental accuracy was poor. Thus, the committee performed a second benchmark in 2006. This time, we carried out scale model tests including flow visualization by using PIV and laser light sheet methods. The numerically predicted flow patterns, local velocity distributions and the intensity of vortices were then compared with experimental results. Matsui (2006) had already reported a part of these results. In this paper, we present the remaining results of the benchmark for the flow and vortices in model sumps.

2. BENCHMARK STUDY

A benchmark study was carried out to survey the computational accuracy and reliability for predicting the likelihood of vortices in sumps by using CFD codes. The computations were done by committee members consisting university faculty members and engineers working for pump manufacturers. The computational results were then compared with experimental ones.

2.1 Model sump and operating conditions

Figure 1 shows the scale model pump sump geometry of the benchmark. Free surface vortices, i.e., air-entrained vortices, and sub-surface vortices, i.e. submerged

vortices, are mainly observed in this sump. The center of the pump is set off a little bit, that is by 3.3% of the sump width, from the center of the sump passage to induce the vortex.

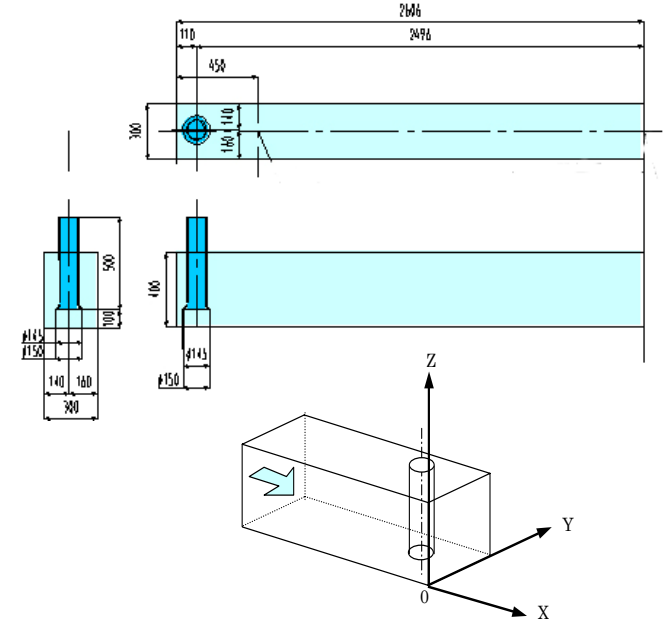


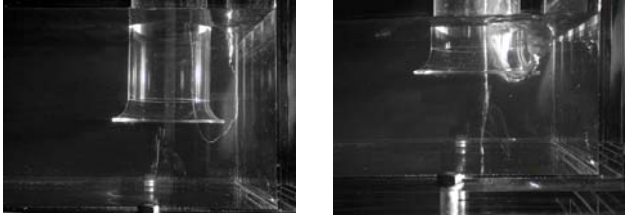
Fig. 1 Scale model pump sump and coordinates for benchmark

2.2 Operating conditions

The benchmark was carried out under three operating conditions concerning flow rate (Q) and submergence (H) (Table 1). These conditions were fixed on the basis of the preliminary experimental results. An air-entrained vortex usually occurs in case 1. Although the cores of these vortices move around and their size varies frequently, the vortices are almost in a steady state. A photograph of this situation is shown in Fig.2 (a), which is a view in the y direction. In case 2, the air entraining is unsteadier, so that the vortex appears and disappears in succession. In case 3, a submerged vortex can be found as a vortex with cavitation bubbles. The air-entraining vortex in case 3 is greater than the submerged vortex and very unstable. Figure 2 (b) shows a photograph of this flow viewed in the y direction. Sometimes there are two air-entraining vortices, for a while there is one, and then there is none.

Table 1 Operating conditions for the CFD benchmark

Case	Flow Rate Q [m ³ /min]	Water level H [mm]	Situation
1	1.0	230	air-entrained vortex (steady)
2	0.6	230	air-entrained vortex(unsteady)
3	1.0	150	Submerged vortex and unsteady air-entrained vortex



(a) Air-entrained vortex (b) Submerged vortex accompanying air-entrained vortex

Fig. 2 Example photographs of visible vortices

2.3 Contributed CFD codes

A total of six committee members participated in the benchmark study. Table 2 shows the characteristics of the contributed CFD codes. The codes consist of commercial CFD codes like STAR-CD 3.22 and 3.26, ANSYS CFX 10.0, Virtual Fluid System, and SCRYU/TETRA V6.

The upstream boundary is assumed to have a uniform velocity distribution, with small turbulence. The measured inlet velocity distribution was reported in the last paper (Matsui 2006). The downstream boundary is set at the $z=600$ [mm] of the suction pipe. All codes treat a single phase flow and the free surface as a fixed ‘slip wall’ without friction. Therefore, the computation does not take into account the deformation of the surface .

2.4 Method of visualizing vortices

As mentioned before, in the TSJ standard for the pump sump model test, the criteria for evaluating the vortex depends on the occurrence of visible vortices. Thus, the CFD technique must also predict whether the calculated vortices will be visible or not, i.e., whether the vortex core is in a gas state or in a liquid state. Since all codes treat a single-phase flow in the CFD computations, the gas phase is not directly predictable. The vortex core diameter is very small compared with the computational grid size. Thus, an additional technique is necessary for predicting visible vortices. Some codes use a stretched vortex model to improve the computing resolution, and the calculated static pressure at the vortex core is compared

with the saturated vapor pressure. Since Shibata (2000) and Iwano (1993) developed this technique and Nagahara applied it (2005), we will not explain it in detail here. A few participants in the benchmark could apply a technique visualizing vortices. Hence, predicting the critical submergence in which the visible vortices start was not a prerequisite condition for the benchmark. Thus, we examined only stream lines or vortex core lines that all participants could obtain by post-processing as alternative methods for detecting visible vortices formed by two phase flows.

3. EXPERIMENTS

3.1 Experimental test scale model

Figure 3 and Fig. 4 show photograph of the test model sump and the schematic diagram of the test loop, respectively. The test section of the flow passage has a



Fig. 3 Test model sump

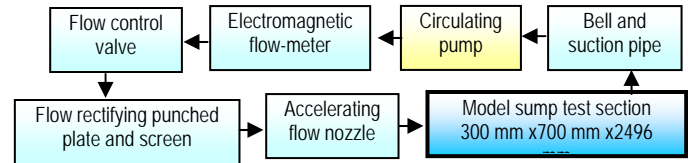


Fig. 4 Schematic diagram of test loop

Table 2 Benchmark codes and conditions

Code	A	B	C	D	E	F
Software	STAR-CD 3.22	ANSYS CFX 10.0	ANSYS CFX 10.0	STAR-CD 3.26	Virtual Fluid System 3D	SCRYU/TETRA V6
Method	finite volume	finite volume	finite volume	finite volume	Vortex method	finite volume
Turbulence model	k-ε/RNG	k-ε	k-ε	k-ε/RNG	(not used)	SST Shear-Stress Transport)
Pre-processor	CADAS	ANSYS CFX 10.0	ANSYS CFX 10.0	Gambit	ANSA	SCRYU/TETRA V6
Post-processor	PRO-STAR FIELDVIEW 10.0	ANSYS CFX 10.0 FIELDVIEW 10.0	CFX-Post10.	PRO-STAR FIELDVIEW 10.0	EnSight	SCRYU/TETRA V6
Grid	non-structured	structured	non-structured	non-structured	Gridless	non-structured
Number of nodes					(surface panels)	
Case 1	2,700,000	1,230,000	100,000	525,000	10,000	1,380,000
Case 2	2,700,000	1,230,000	100,000	224,000	10,000	1,380,000
Case 3	2,100,000	1,220,000	80,000	358,000	10,000	1,150,000

rectangular shape, and it is constructed from transparent acrylic resin for visualization and optical measurements. The uniformity of the inlet flow is obtained by an accelerating the flow nozzle, rectifying the punched plates, and installing honeycomb plates upstream of the test section. The clearance between the bell and the bottom surface is set as 100 mm, i.e., two thirds the height of the bell diameter. The water is sucked by a suction pipe with the bell and is sent to the circulating head by a centrifugal pump with a speed control. The flow rate was measured using an electromagnetic flow meter.

3.2 Experimental instruments and procedure

The items shown in Table 3 were measured by each instrument. The PIV and LLS methods were applied for the cross sections shown in Table 4. The suction vortex phenomena were observed at least 10 min at each measuring condition. Because, according to the TSJ standard, the observing time is 10 minutes in the most severe criteria. The characteristic vortex duration T2 and time period T1 (Fig. 7) were visually measured.

Table 3 Measuring instruments

Instruments	Measuring items	Specifications
Video camera, Still camera	Features of suction vortices	Digital video camera
PIV	Flow pattern, Velocity vector, Vorticity	YAG Laser (523nm) Video:30f/s, 1024x1024 pixel, TSI, PIVCAM10-30, Model630046 Laser Pulse Model 610034
Laser light sheet	Stream line, Location of vortex core	Solid-state laser Chopper

Table 4 Measuring sections for LLS and PIV

Section	Ordinates	Explanation
X110	X=110mm, parallel to YZ plane	Vertical cross section through the pump center
Y010	Y=10 mm, parallel to XZ plane	Vicinity of the side wall
Y140	Y=140mm, parallel to XZ plane	Vertical cross section through the pump center
Z010	Z=10 mm, parallel to XY plane	Parallel and close to bottom surface
Z085	Z=85mm, parallel to XY plane	Parallel and close to the pump bell
Z220	Z=220mm, parallel to XY plane	Parallel and close to the water surface

4. COMPARISON OF COMPUTATIONAL AND EXPERIMENTAL RESULTS

4.1 Observed vortices and critical submergence of the visible vortices

The typical observed vortices are shown in Fig. 2. Figure 5 shows the region of the flow rate and water level, where the visible vortices are observed. The points indicating the three cases of the benchmark are also shown

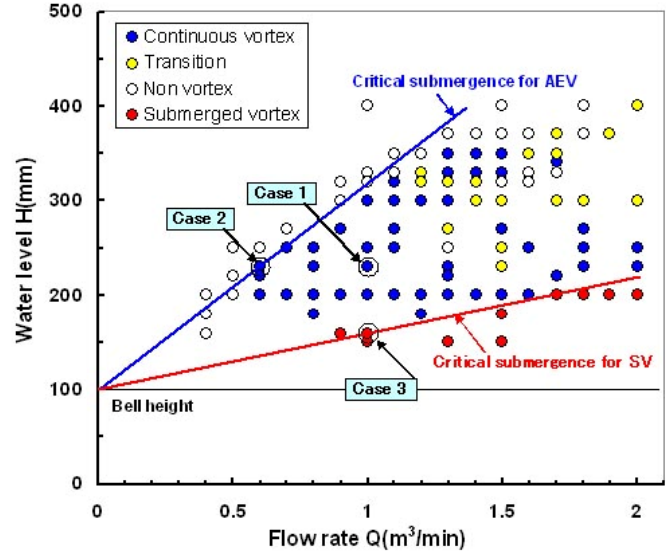


Fig. 5 Suction vortex generating region of flow-rate and water level

in the figure. It was found that the critical submergences for the air-entrained vortex and submerged vortex have approximately linear relationships with the flow rate. But the critical submergence diverges from the line at large flow rates and higher water level. This is caused by the high surface wave occurring behind the suction pipe. This wave breaks the stable vortex and suppresses the occurrence of the air entrained vortex. Predicting the critical submergence is not obliged in the benchmark. Hence, the predicted submergence is not shown in Fig.5. If the CFD technique becomes an alternative method for evaluating sump performance, it will become necessary to predict the critical flow rate and water level where visible vortices occur. Hence, an accurate CFD predicting method should be developed soon.

Figure 6 shows one of the unsteady characteristics of

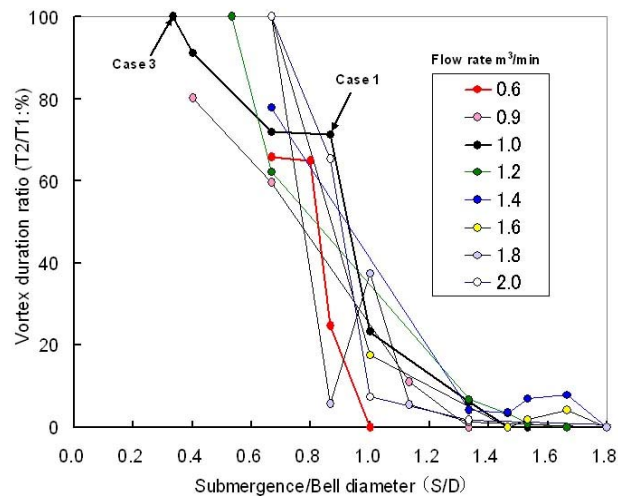


Fig. 6 Relation between vortex duration and submergence

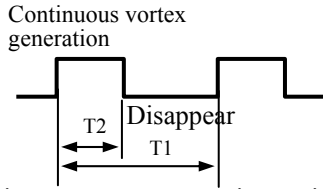


Fig. 7 Continuous vortex generating period and its duration air-entrained vortices, that is, the relationship between normalized submergence and time ratio of the vortex duration and period. The parameter shows the flow rate. Time duration T_1 and period T_2 are indicated in Fig.7. The

value of $T_2/T_1=100\%$ means that the vortex occurs all the time. We found that the visible vortex rapidly appears and disappears around at submergence ratio=0.8 to 1.0. Since suction vortices have unsteady characteristics, an unsteady CFD computation is necessary to predict the occurrence of suction vortices and we set the benchmark of case 2 for the unsteady vortex. However, we have too much data from the unsteady CFD calculation and we don't have a reasonable evaluation method for the computational results yet. Space is too limited for a full explanation in this paper. Hence, we eliminate the explanation of the results of case 2.

Table 5 Comparison of stream lines calculated by each code

Case 1 Streamline			
Code A		Code B	
Code C		Code D	
Code E		Code F	

Table 6 Comparison of vortex core lines calculated by each code

Case 1 Vortex core line			
Code A		Code B	
Code C		Code D	
Code E		Code F	

4.2 Flows in the model sump

1) Stream line and vortex core line

Table 5 shows the stream lines obtained by computations based on each CFD code in case 1. Complex stream lines containing vortex flow patterns are shown in each figure. Some vortex stream lines entering the pump bell are observed on the water surface in the results for Code A, Code B, Code D, and Code E. The air-entrained vortex occurs in the area behind the pump suction pipe and nearer to the z-axis shown in Fig. 1. Three and two vortices are observed on the water surface in the results of Code B and Code A, respectively. But as shown in Fig. 2, only one continuous air-entrained vortex occurs. Hence, it is difficult at present to evaluate the occurrence of a visible air-entrained vortex only with the stream lines obtained by the computation. Some post-processing programs have the function to detect the vortex core. Table 6 shows the results of such a detection. The center of the vortex core is visualized as lines. The color bar indicates the magnitude of vorticity. According to these vortex core lines, we can approximately see the situation of the vortex in the sump. Each figure shows many vortex core lines. But as mentioned above, only one air-entraining vortex was observed in case 1. If we apply the computational core line for predicting the visible vortices, we have to consider the critical value of vorticity. Only core lines having vorticities over a critical value will be visible. Therefore, the critical vorticity for a visible vortex should be determined experimentally or theoretically.

An additional post-processing such as obtaining the vortex core static pressure and comparing it with the ambient pressure for an air-entrained vortex or the saturated vapor pressure of water for a submerged vortex would be necessary to predict the visible vortices. Iwano (1993) and Shibata (2000) developed such a technique that can work in most of the above situations .

2) Locations of vortices

Figure 8 shows the locations of the center core of air-entrained vortices on the free surface, obtained by

computations and experiments for case 1. Many air-entrained vortex core locations were obtained by using the laser light sheet method (Fig.9). The average location is indicated in Fig. 8 as the “Air entrained” circular point. We can see the following results by comparing these figures. Almost all of the computational codes predicted the location of the air-entraining vortex well. They also predicted that other vortices will occur in the upper area behind the suction pipe. However, only one visible air-entrained vortex was observed experimentally. Figure 10 shows the predicted locations of the air-entrained vortex and submerged vortex in case 3. Figure 11 shows only experimentally measured locations of air-entrained vortices and submerged vortices in case 3. As mentioned before, both the air-entrained vortex and submerged vortex occur in this case and two groups of air-entrained vortices are generated behind the suction pipe. Their locations are scattered much more widely than the results of Fig. 9. This means the air-entrained vortices in case 3 are less steady than in case 1. One can see this from the fact that Code B predicted much more vortices than were observed. It is beyond our expectation that the observed locations of the submerged vortices spread wide vertically in the circle of the suction pipe. The submerged vortex may be greatly interfered with unsteady air-entrained vortices. Thus, we

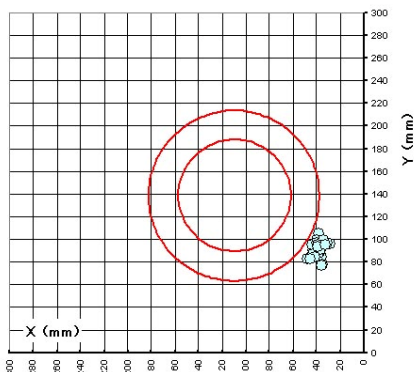


Fig. 9 Measured location of air-entrained vortex core at water

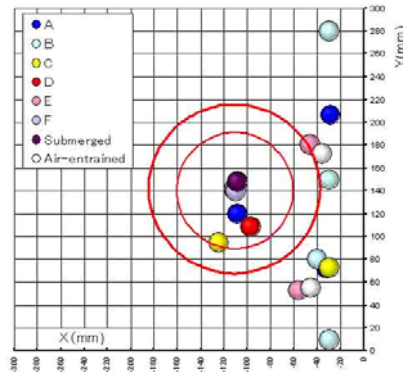


Fig. 10 Predicted and measured location of air-entrained vortex core and submerged vortex core in Case 3

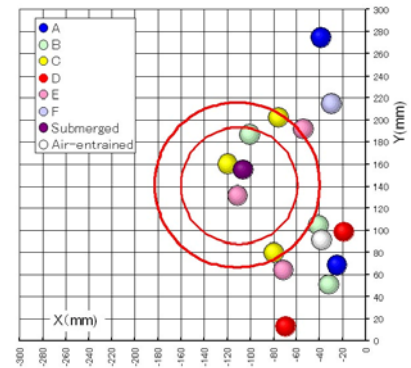


Fig. 8 Predicted and measured location of air-entrained vortex core at water surface in Case 1

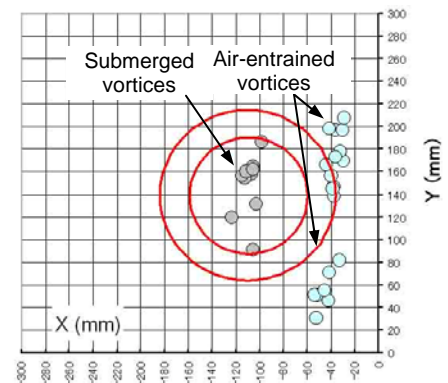


Fig. 11 Measured location of air-entrained vortex core and submerged vortex core in Case 3

can conclude that most CFD codes are able to simulate the suction vortex location well, except vortex number.

3) Velocity vector

Table 7 shows the computational and experimental velocity vectors in case 1 at section Y140 which is the cross section including the suction pipe center line and parallel to the side wall. The photograph of stream lines obtained with the laser light sheet method and the PIV results are also listed. The color scales of the figures are all the same as velocity 0 to the maximum of 1.5 m/s except for the PIV result. We can not find any remarkable differences among these figures. We can see that the flow enters the bell smoothly without disturbance. An air-entrained vortex occurs occasionally in this area. But except for the result of Code C, no signs of vortex flow are observed in the region between right side of the suction pipe and the back wall of the sump. The suction vortex

may occur in a fairly small area. Table 8 shows the velocity vectors obtained numerically and experimentally in case 1 at section Z220. This section is located just under the water surface. We can see the following from these figures. The vortex flow patterns are observed in the figures of Code A, Code D, Code E, and Code F. The vortex stream line and vortex core line obtained by Code B are clearly shown in the figures of Table 5 and Table 6. However, no vortex flow pattern is visible in the figure of Code B of Table 8. The cause is that the diameter of the air-entraining vortex and its intensity are small.

Table 9 compares the velocity vectors obtained numerically and experimentally in case 3 at section Z010. This section is close to the bottom surface of the sump. In this case, the submerged vortex occurs in the vicinity of the circular pipe center as shown in Fig. 2(b). The vortex flow patterns are observed in each figure except for the

Table 7 Calculated and measured velocities at section Y140

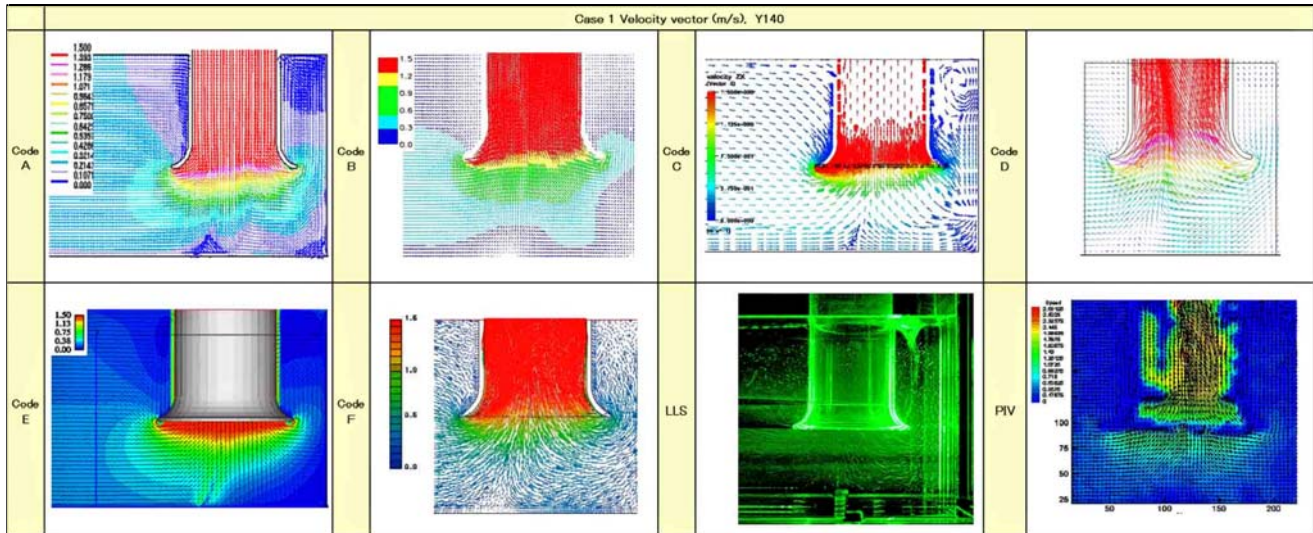


Table 8 Calculated and measured velocities at section Z220

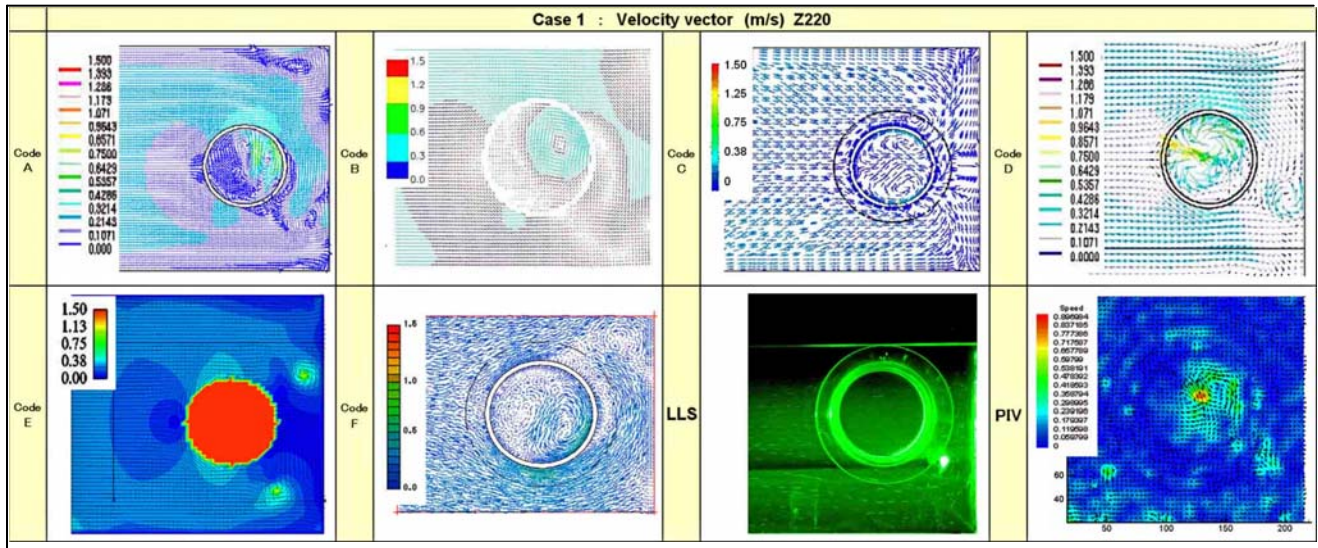


Table 9 Calculated and measured velocities at section Z10

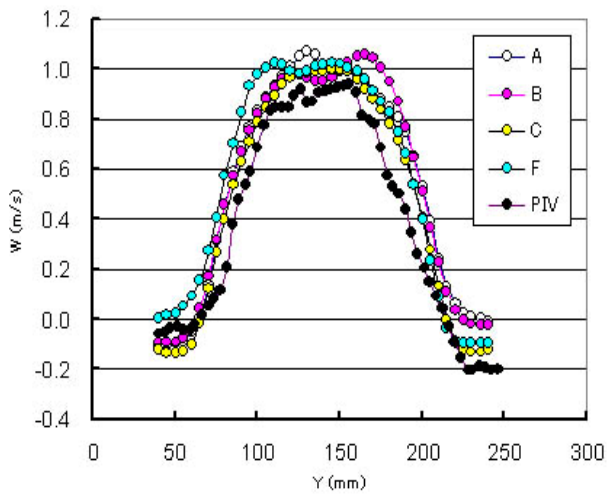
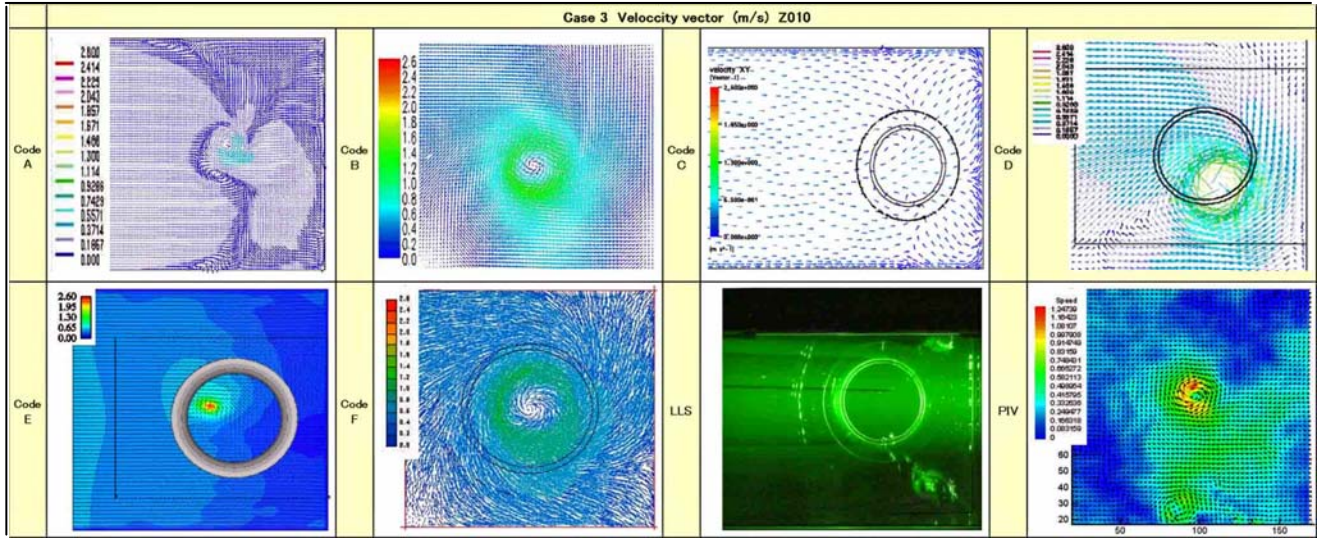


Fig. 10 Velocity w distribution at bell inlet section Z085

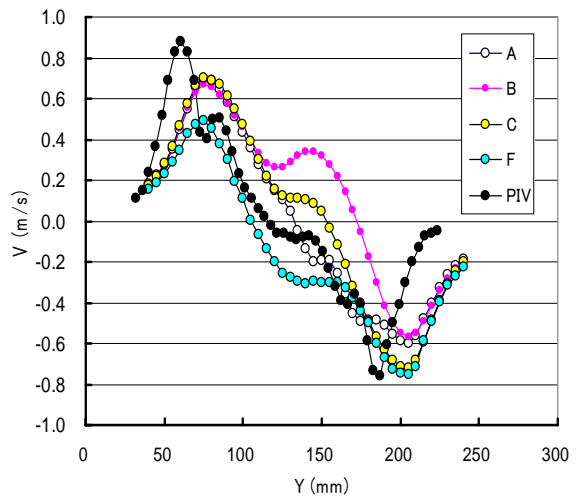


Fig. 11 Velocity v distribution at bell inlet section Z085

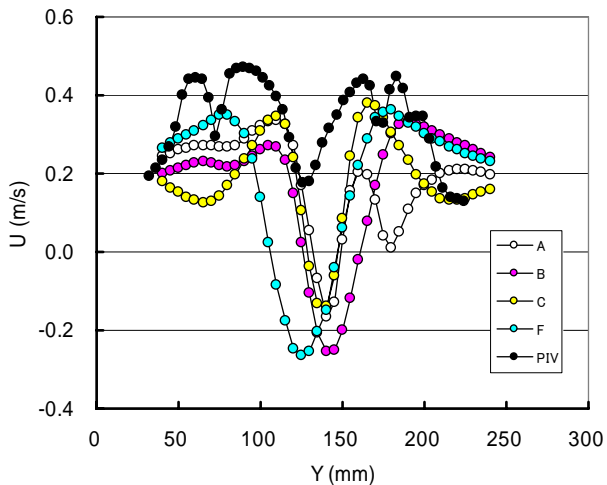


Fig. 12 Velocity u distribution at bell inlet section Z085

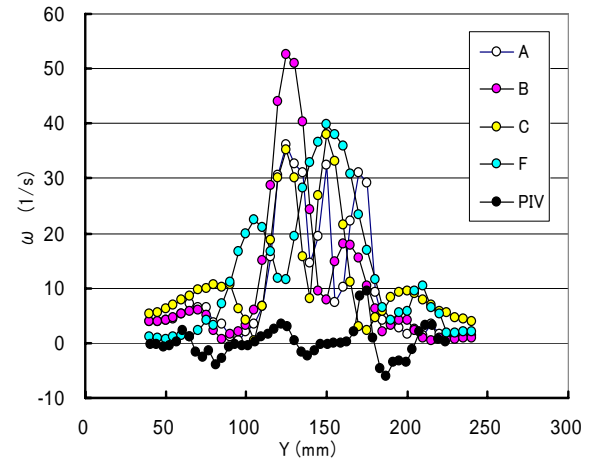


Fig. 13 Vorticity ω distribution at bell inlet section Z085

result of Code C. There are no signs of the vortex flow pattern in the figure of Code C. The maximum velocities in the vortex predicted by Code A, Code B, and Code F are almost the same as the one measured by the PIV (1.25 m/s). However, the value predicted by Code E is nearly twice the measured one. Since Code E is an analytical method, which has an advantage in unsteady flow simulations, the maximum velocity it calculates may have a higher accuracy than the other codes' values. If the PIV method is used to measure unsteady vortex flow, the average measured velocity may decrease, because the vortex center fluctuates and the upper and lower peak velocities are averaged; Hence the velocity distribution in the vortex changes from a sharp pattern to a dull one. Nagahara (2003) already pointed out this phenomenon.

Figures 10 to 12 show the velocity distributions at the

bell entrance along the bell diameter in the y direction. w , v , u means the velocity components in the z , y and x directions, respectively as shown in Fig. 1. The axial flow velocity distributions calculated by each code mostly agree with the PIV measured result. Each predicted v distribution agrees qualitatively with the experimental PIV result. However, there is a great difference in the u distributions. This may be caused by the PIV method's lack of measuring accuracy for u .

4) Vorticity

Table 10 and Table 11 respectively show the vorticity distribution at section Z220 for case 1 and at section Z010 for case 3. We can see the following. The high vorticity region is not observed outside of the suction pipe circle in the figures of Code B and Code C of Table 11. The magnitude and contour pattern of the vorticity varies

Table 10 Calculated and measured vorticities at section Z220

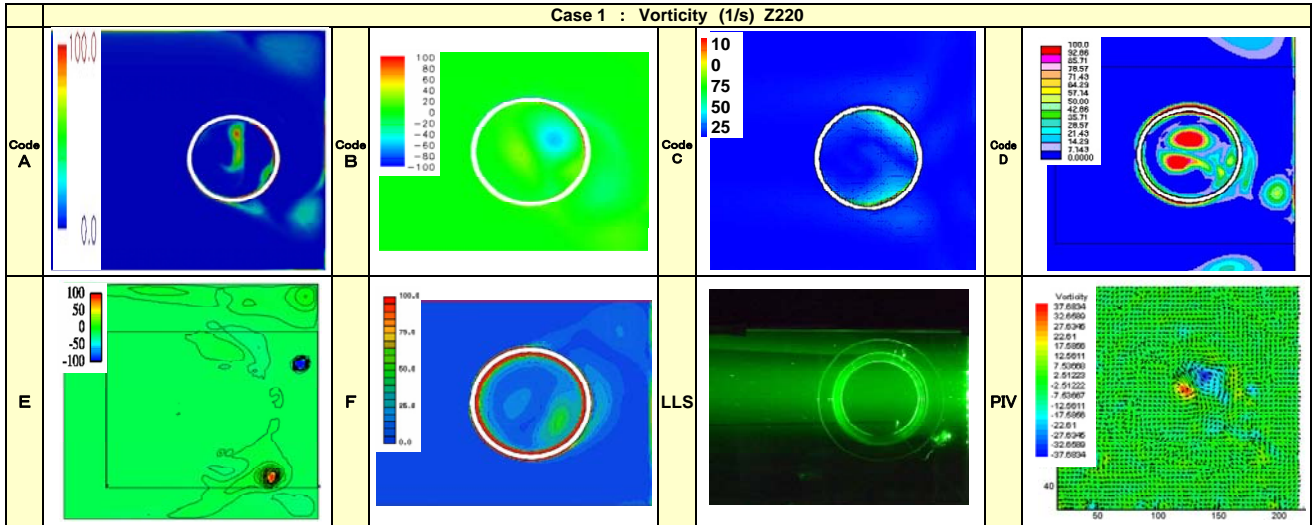
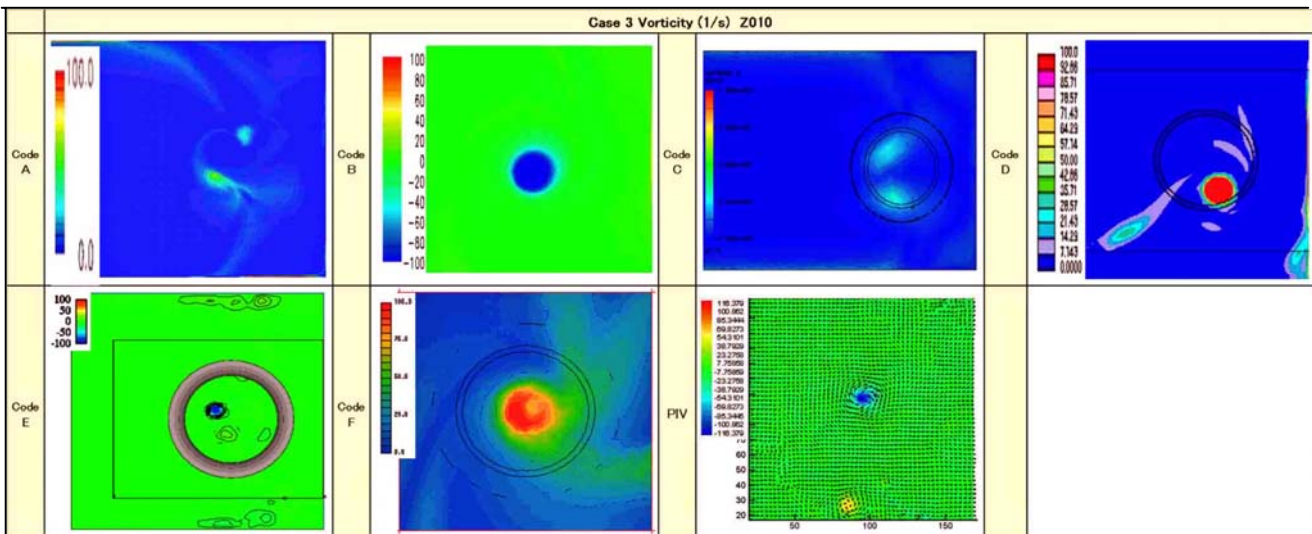


Table 11 Calculated and measured vorticities at section Z010



widely with each code. This is confirmed from Fig.13 showing the vorticity distribution along the bell diameter. The PIV measurement result is very small. As mentioned above, this is caused by that the experimental vorticity is calculated from the average velocity but the instantaneous velocity should be used instead (Nagahara 2003). We can see in Table 12 that the local vorticity in the suction pipe is greater than of the value outside of the pipe. Hence, we confirmed that the vorticity of the air-entrained vortex near the free surface becomes greater in the suction pipe.

5. CONCLUSIONS

A benchmark test was carried out for the flow field and suction vortices in a pump sump model. The following results were obtained.

- 1) The critical submergence for the air-entrained vortex is almost proportional to the flow rate in the sump. The vortex behavior is unsteady, and the duration of the vortex varies greatly.
- 2) The submerged vortex appears accompanying the air-entrained vortex in the region of low submergences and high flow rates. The critical submergence for the submerged vortex is also proportional to the flow rate.
- 3) Some CFD codes can predict the visible vortex's occurrence and its location for submergence and flow rate conditions with enough accuracy for industrial use.
- 4) The calculated velocity distribution at the bell entrance qualitatively agrees with the experimental results. However, the agreement is poor in terms of the magnitude and distribution patterns of the vorticity. This difference is caused by the lack of accuracy of the experiment and CFD computation.
- 5) Predicting the critical submergence for visible vortices was not imposed in the benchmark. The calculated stream lines and vortex core lines are not able to be used to predict the visible vortices. An additional post-processing such as obtaining the vortex core static pressure and comparing it with ambient pressure for an air-entrained vortex or with the saturated vapor pressure of water for the submerged vortex would be necessary to predict the visible vortices.

ACKNOWLEDGMENTS

This study was performed by members of the Research Committee on Pump Sump Model Testing of Turbomachinery Society of Japan. We are grateful to the following committee members for their providing their results and valuable advice. We would especially like to thank Dr. Akira Manabe for his organizing of the CFD results. We also would like to express our thanks to Mr. Kazuma Suzuki and Mr. Takaaki Hirasawa of Yokohama National University for their help in the experiments.

**The Research Committee on Pump Sump Model
Testing of Turbomachinery Society of Japan**

Chairman: Prof. Kyoji Kamemoto, Yokohama National University, Secretaries: Dr. Tomoyoshi Okamura and Associate Prof. Jun Matsui, Yokohama National University, Members: Prof. Toshiaki Ikohagi, Tohoku University, Prof. Hiroshi Tsukamoto, Kyushu Institute of Technology, Dr. Kazuo Uranishi, Hachinohe National College of Technology, Mr. Koji Nomura, Tokyo Metropolitan Government, Dr. Tatsuo Naka, National Institute for Rural Engineering, Mr. Teruyuki Miyauchi, Association of Pump System Engineering, Mr. Kenji Kawakita, Public Works Research Institute, Dr. Yuzuru Eguchi, Central Research Institute of Electric Power Industry, Mr. Motoaki Shiobara, Tokyo Electric Power Company, Mr. Akio Ido, DMW Corp., Mr. Hiroyuki Yamamoto, Kubota Corp., Dr. Akira Manabe, Hitachi Plant Technologies, Ltd. Dr. Takahide Nagahara, Hitachi Plant Technologies, Ltd., Mr. Kou Fujino, Ebara Yoshikura Hydro-Tech Co., Ltd., Dr. Hideaki Maeda, Torishima Pump MFG. Co. Ltd., and Mr. Hiroshi Kawane, Mitsubishi Heavy Industries, Ltd.

REFERENCES

- Ansar, M., Nakato, T. and Constantinescu, G., 2002, "Numerical simulations of inviscid three-dimensional flows at single-and dual-pump intakes", *Journal of Hydraulic Research*, Vol. 40, No. 4, 461-470.
- Iwano, R., 1993, "Onset Condition of Vortex-Induced Gas Entrainment at Free Surface", *Proc. of Japan Society of Mechanical Engineers*, No. 930-9, pp. 594-596, (in Japanese).
- Matui, J., Kamemoto, K. and Okamura, Tomoyoshi, 2006, "CFD Benchmark and a Model Experiment on the Flow in Pump Sump", *Proc. of 23rd IAHR Symposium-Yokohama*.
- Nagahara, T., et al., 2003, "Measurement of the Flow around the Submerged Vortex Cavitation in a Pump Intake by Means of PIV", *Proc. Fifth International Symposium on Cavitation (Cav 2003)*, Cav03-OS-6-011, Osaka, Japan.
- Okamura, T. and Kamemoto, K., 2005, "CFD Simulation of flow in model pump sumps for detection of vortices", *Proc. of 8th Asian International Fluid Machinery Conference*, Yichang, China.
- Rajendaran, V.P., Constantinescu, G.S. and Patel, V.C., 1998, "Experiments on Flow in a Model Water-Pump Intake Sump to Validate a Numerical Model", *Proc. of FEDSM'98, ASME Fluids Engineering Division Summer Meeting*, June21-25, Washington, DC.
- Shibata, T., Iwano, R., Nagahara, T. and Okamura, T., 2000, "A Numerical Method for Predicting the Cavitation Inception of a Submerged Vortex in a Pump Sump", *Proc. of 20th IAHR Symp.*, August 6-9, Charlotte, North Carolina, U.S.A., CFD-G03 (2000).
- The Turbomachinery Society of Japan, 2005, TSJ Standard S002:2005 "Standard Method for Model Testing the Performance of a Pump Sump" (in Japanese).